# Mode Splitting and Resonant Coupling between a Slot Metasurface and PMMA

Michael F. Finch[a], Brian A. Lail[a]
[a]Department of Electrical and Computer Engineering, Florida Institute of Technology, 150 West University Blvd., Melbourne, FL USA 32901

## ABSTRACT

A slot metasurface (metascreen) designed to have resonance that couples with the 1733 $cm^{-1}$ absorption peak of the C=O molecular bond of PMMA (polymethyl methacrylate) is presented. The metasurface is made of a gold layer perforated with periodically-placed slots and stood off above a reflective ground plane with silicon substrate. The metasurface is modeled using ANSYS HFSS and including measured optical properties for gold, silicon and PMMA in the infrared spectrum. PMMA forms a thin overcoat and exhibits a strong absorption resonance at wavenumber 1733 $cm^{-1}$. Coupling between the metasurface and PMMA is observed via normal mode splitting. Mode splitting has been analyzed from classical coupled mass spring oscillators to exciton-photons coupling in microcavities. The coupled systems can be described with a Hamiltonian matrix and solved for the eigenfrequencies. Parametric analysis of coupled response as a function of the design geometry is provided. Coupling energy, reflectance spectrum, and dispersion plots showing the anticrossing behavior of hybrid modes are presented as characterization of resonance coupling and normal mode splitting. Slot metasurface results are compared to the complementary structure (nanorod metasurface) in order to explore the duality of the complentary metasurfaces and their coupled responses. Coupled resonances have application in biosensors for molecule detection, surface-enhanced infrared absorption (SEIRA), and infrared imaging.

**Keywords:** Metasurface, Normal Mode Splitting, PMMA, Resonant Coupling

## 1. INTRODUCTION

Metamaterials are patterned structures that give rise to effective bulk material properties[1, 2]. A planar metamaterial is a specific subcategory that is referred to as a metasurface. Metasurfaces are appealing structures due to the maturity of VSLI fabrication technology and processes. There are applications of metasurfaces in sensing region, where said structures are coupled with some form of unknown material. An example system can be seen in Figure 1 where surface-enhanced infrared absorption (SEIRA) based system is used. Evidence of coupling can be seen from a scattered spectrum that then can be detected. The coupling event has been referred to as vacuum Rabi splitting, quantum level repulsion, level anti-crossing, or normal mode splitting. The latter term will be used in naming the coupling event. Polymethyl methacrylate (PMMA) is used here as a stand-in for the unknown material to which a metasurface will be designed to couple. The PMMA material is appealing since it is a readily available photoresist which is already well characterized in the IR band of interest. PMMA has an IR absorption peak at approximately 52 THz (1733 $cm^{-1}$ or 5.77μm). The absorption peak is correlated to the phonon or vibrational moments of the carbon double bonded with oxygen bond in the chemical structure of the material. ANSYS HFSS is used to design a resonance metasurface to couple with the PMMA C=O bond. This coupling will be evidenced via the normal mode splitting.

Resonance-coupled metasurfaces have profound applications with SEIRA[3-6], Surface-enhanced Raman spectroscopy (SERS)[7-9], and biosensing[10]. This paper investigates the coupling event in a periodic planar meta-slot structure with the 52 THz phonon moment. The results of slot metasurface will then be compared with results of a nanorod metamaterial presented in reference [5]. The complentary principle in the field of optics was introduced by Babinet and was expanded upon by Booker[2, 11-13]. Babinet's principle for diffraction pattern of complentary screens will be discussed in terms of the two metasurfaces.

Photonics Applications for Aviation, Aerospace, Commercial, and Harsh Environments V,
edited by Alex A. Kazemi, et. al., Proc. of SPIE Vol. 9202, 92021B · © 2014 SPIE
CCC code: 0277-786X/14/$18 · doi: 10.1117/12.2062173

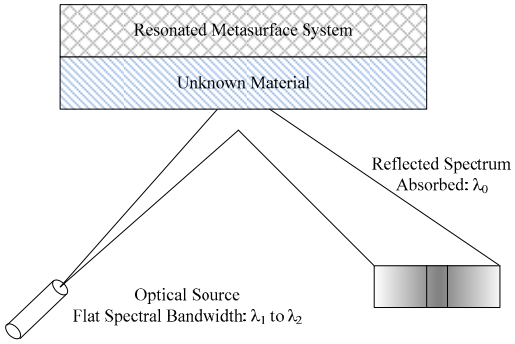


Figure 1. SEIRA based sensor utilizing a resonate metasurface to enhance the reflected signal.

## 2. Design Process

The model of the metasurface with PMMA overlay is shown in Figure 2. The model contains a PEC ground plane, a silicon cavity, gold metascreen with a slot of orders of microns in length, and the PMMA overlay. The model, Figure 2, is a unit cell of a periodic structure which when simulated will model an array of nanoslots. The model uses measured material optical properties in the simulation in order to produce the normal mode splitting. The metasurface was designed with the aid of an auxiliary model with "dummy" PMMA overlay. The PMMA "dummy" is a dispersionless stand-in which assists in identifying any red/blue shifting of the metasurface's resonance.

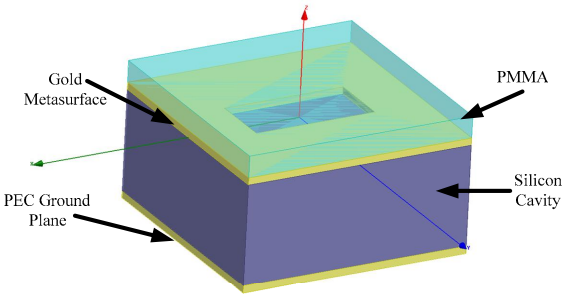


Figure 2. Nanoslot metasurface unit cell designed in HFSS.

The HFSS model with the dispersionless material is tuned via the Si cavity (depicted in Figure 2). The uncoupled red-shifted metamaterial is tuned to the desired 52 THz resonant frequency. The metasurface resonates with the phononic moment in the PMMA which results in coupling.

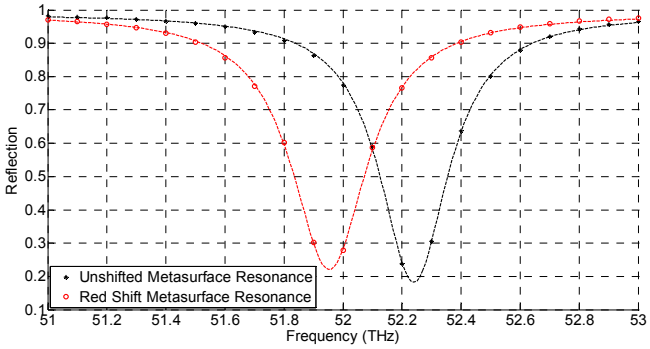


Figure 3. Reflected spectrum for red shift and unshifted, uncoupled resonances showing approximately 0.2 THz red shift.

The coupling of the two resonances may be described by a Hamitonian matix[5, 14] which can be solved for the eigenfrequency of the coupled system.

$$H = \hbar \begin{bmatrix} \omega_1' - j\gamma_1 & V \\ V & \omega_2' - j\gamma_2 \end{bmatrix} \quad (1)$$

In Equation 1 $\omega_n$' is the red-shifted uncoupled resonances, $\gamma_n$ is the damping or loss of the uncoupled resonances of metasurface/PMMA, and *V* would relate to the coupling strength between the two resonances. The eigenfrequencies can be calculated using the determinant as follows: det(H-ħωI) = 0. The solved equation becomes as follows:

$$(\omega_1' - \omega - j\gamma_1)(\omega_2' - \omega - j\gamma_2) - V^2 = 0 \quad (2)$$

Equation 2 solution is well known from the exciton-polariton description of normal mode splitting[15]. As such the complex solutions for the eigenfrequencies are:

$$\omega\pm = \frac{\omega_1'+\omega_2'}{2} - \frac{j}{2}(\gamma_1+\gamma_2) \pm \sqrt{\left(\frac{\omega_1'-\omega_2'}{2}\right)^2 + V^2 - \left(\frac{\gamma_1-\gamma_2}{2}\right)^2 + \frac{j}{2}(\omega_1'-\omega_2')(\gamma_1-\gamma_2)} \quad (3)$$

The quantity ($\omega_1$' – $\omega_2$') is known as detuning in vacuum Rabi splitting terms and the term "δ" is used. Simplifying assumptions will be imposed onto Equation 3. First, the in the spectrum region of interest the detuning is very small, i.e., $\delta \approx 0$, and thus the eigenfrequencies are real. It would be appealing to have the coupling constant in terms of modeled results. The difference between the ω+ and ω-, i.e., the difference in the coupled eigenfrequencies will be defined as $2\Omega_r$ when $\delta \Rightarrow 0$ (depicted in Figure 4). Then using the first assumption, an equation for the coupling constant is as follows:

$$V^2 = \Omega_r^2 + \left(\frac{\gamma_1-\gamma_2}{2}\right)^2 \quad (4)$$

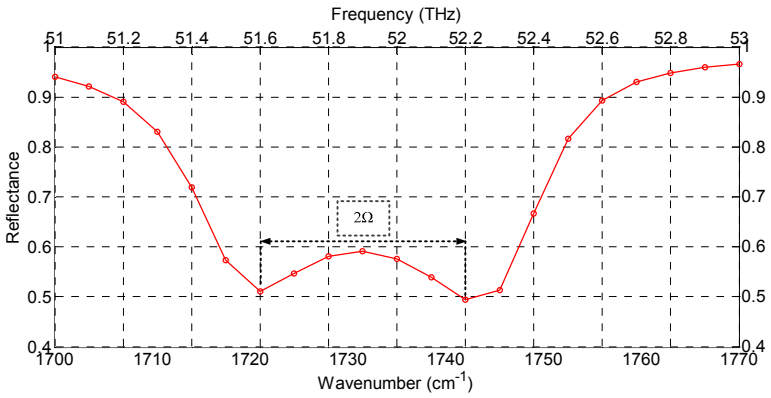


Figure 4. Reflection spectrum depicting the Rabi splitting value.

The quantity $\hbar\Omega_r$ is referred to as Rabi energy which describes the energy difference between the hybrid or splitted energy levels[4, 5, 14]. From Equation 4 the second assumption can be drawn. The damping or $\gamma_n$ is related to the full width haft maximum (FWHM) of the uncoupled resonance[16] so, it will be assumed that the resonances are "well matched", i.e., $|\gamma_1-\gamma_2| \approx 0$. From the two assumptions Equation 3 can be rewritten as:

$$\omega\pm \approx \frac{\omega_1'+\omega_2'}{2} \pm \sqrt{\left(\frac{\omega_1'-\omega_2'}{2}\right)^2 + {\Omega_r}^2} \quad (5)$$

## 3. Results

The thickness of the silicon cavity seen in Figure 2 is tuned to where maximum coupling occurs, which is labeled Nominal Case in Figure 5. The silicon cavity is tuned around the nominal case by 200nm as depicted in Figure 5. The data shown in Figure 5 was fitted with a double Lorenzian as seen in Equation 6[1].

$$r(\omega) \approx -j\left[\frac{a_1}{(\omega-\omega_1)+j\gamma_1} + \frac{a_2}{(\omega-\omega_2)+j\gamma_2}\right] \quad (6)$$

In Equation 6, $\omega_n$ correspond to dips in the reflection coefficient, $\gamma_n$ represent the losses, and $a_n$ are amplitude scaling coefficients.

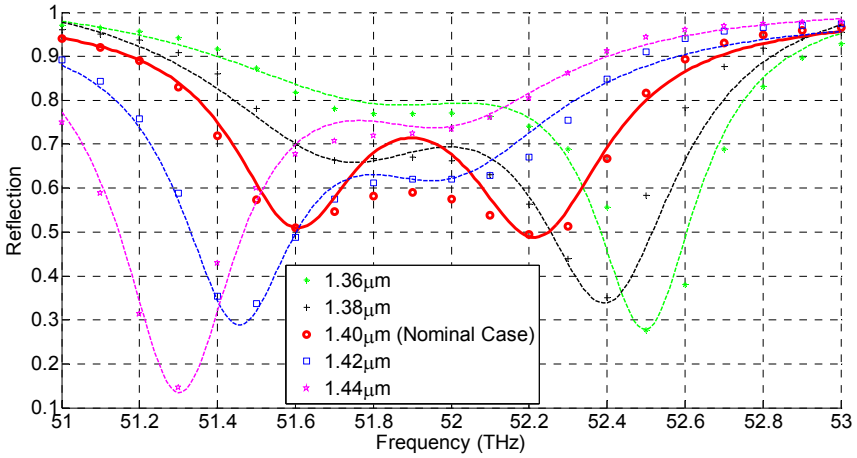


Figure 5. Reflection spectrum HFSS modeled results for coupled metasurface and PMMA resonances.

Fano resonance[17, 18] and electromagnetic induced transparency (EIT)[1, 19, 20] are two different phenomenon that have been used to explain the lineshape of the nominal case. Fano resonance in a quantum sense is the interaction of a continuum of states with a bound state which then results in asymmetric lineshapes[18]. In the system the plasmonics would be analogous to the continuum of states and the bound state would be the PMMA's resonance at 52 THz. EIT can be thought of as a special case of Fano resonance where the detuning, δ, is zero or when the uncoupled (shifted) resonances are equal.

Using Equation 5 a dispersion plot of metamaterial resonance and eigenfrequencies of the hybrid modes can be obtained as seen in Figure 6. The Rabi energy is obtained from Figure 5 which is calculated to be 1.24 meV. It will be assumed that there is a negligible shift in the PMMA uncoupled resonance and a 0.2 THz red shift, seen in Figure 3, in the metasurface resonance. Figure 6 has three light lines for uncoupled PMMA, metasurface, and red shifted metasurface resonance.

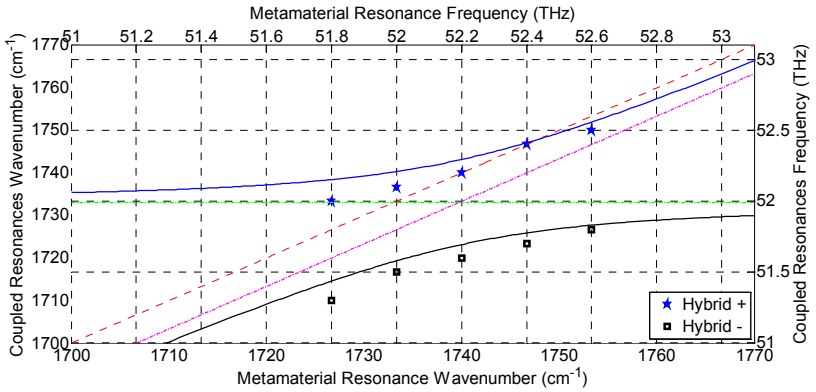


Figure 6. Dispersion curve displaying typical anti-crossing behavior of coupled hybrid modes compared to modeled results.

The resonance peaks for both hybrid modes from Figure 5 are mapped onto the expression of Equation 5 in Figure 6. The mapped resonance peak follows the level repulsion trend that is expressed by Equation 5. The resonant data points are not perfectly on top of the anti-crossing curve. The imperfections may be results of complex coupling frequency which would result in damping or decoupling. Also, practically the PMMA resonance may shift slightly due to the layering of materials and lossy IR metals.

## 4. Conclusion

Consider a slot metasurface designed with the same dimension as a rod metasurface discussed in reference [5]. The resulting reflection coefficient is shown in Figure 7. It can be seen that there is a blue shift in the metasurface resonance that results in similar coupling as that seen in the1.36 μm silicon cavity case in Figure 5. Babinet's principle classically has been confined to infinity thin perfectly conducting planes. Under the classical constrains of Babinet's principle the reflection for the slot or rod would be identical for the appropriate complementary mode, i.e., electric field polarized across the slot or along the rod respectively. However, deviations have been reported[11-13] from classical Babinet's principle under the condition for complementary screens etched onto substrates. The deviation is, more or less, shifts in the resonant peak similar to what is observed in comparing Figures 5 and 7. For design purposes, it would be palatable to obtain, at a minimum, empirical relationships between shifts in resonance in complementary complex structures and parameters of that said structure.

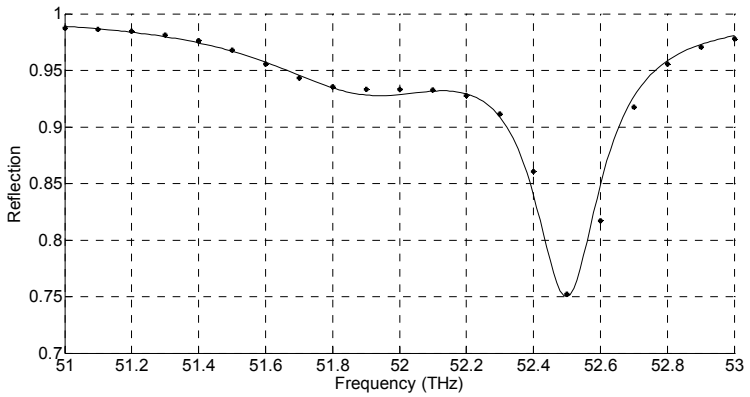


Figure 7. Slot metasurface reflection spectrum will complemtary rod metasurface dimensions[5].

Normal mode splitting has been shown for a slot metasurface with a PMMA overlay. Normal mode splitting is a result of coupling between C=O molecular bond and the slot metasurface resonances. Also, it can be seen from Figure 5 that there is an enhancement of the C=O PMMA moment which correlates with detection applications. Such applications include biosensing and SEIRA or surface-enhanced infrared spectroscopy. A practical analytical model for normal mode splitting is compared to the results produced by finite element analysis.

## REFERENCES


[1] Khanikaev, A. B., Wu, C., and Shvets, G., "Fano-resonant metamaterials and their applications," Nanophotonics, 2(4), 247-264 (2013).

[2] Balanis, C. A., [Advanced Engineering Electromagnetics, Second Edition] John Wiley & Sons, Inc., Hoboken, NJ, (2012).

[3] Chen, K., Adato, R., and Altug, H., "Dual-band perfect absorber for multispectral plasmon-enhanced infrared spectroscopy," ACS Nano, 6(9), 7998-8006 ( 2012).

[4] Shelton, D. J., Brener, I., Ginn, J. C., Sinclair, M. B., Petters, D. W., Coffey, K. R., and Boreman, G. D., "Strong coupling between nanoscale metamaterials and phonons," ACS Nano Letters, 11(5), 2104-2108 (2011).

[5] Finch, M. F. and Lail, B. A., "Modeling of resonant coupling between infrared nanowire metasurface and phonons in pmma," in [The 30$^{Th}$ Annual Review of Progress in Applied Computional Electromagnetics, Computational Methods in Nanoelectromagnetics], (March 23-27, 2014)

[6] Pucci, A., Neubrech, F., Weber, D., Hong, S., Toury, T. and de la Chapelle, M. L., "Surface enhanced infrared spectroscopy using gold nanoantennas," Physica Status Solidi B, 247(8), 2071-2074 (2010).

[7] Vendrell, M., Maiti, K. K., Dhaliwal, K. and Chang, Y. T., "Surface-enhanced raman scattering in cancer detection and imaging," Trends in Biotechnology, 31(4), 249-257 (2013).

[8] Zavaleta, C. L., Kircher, M. F., and Gambhir, S. S., "Raman's ‘effect’ on molecular imaging," The Journal of Nuclear Medicine, 52(12), 1839-1844, (2011).
[9] Jackson, J. B., and Halas, N. J., "Surface-enhanced raman scattering on tunable plasmonic nanoparticle substrates," Proceeding of the National Academy of Sciences of the United States of America, 101(52), 17930-17935 (2004).
[10] Chen, T., Li, S. and Sun, H., "Metamaterials Application in Sensing," Sensors, 12(3), 2742-2765 (2012).
[11] Falcone, F., Lopetegi, T., Laso, M. A. G., Baena, J. D., Bonache, J., Beruete, M., Marque´s, R., Martı´n, F., and Sorolla, M., “Babinet principle applied to the design of metasurface and metamaterials,” Physical Review Letters. 93(19), 197401-1-4 (2004).
[12] Compton, R. C., Whitbourn, L. B., McPhedran, R. C., “Strip grating at a dielectric interface and application of babinet’s principle,” Applied Optics. 23(18), 3236-3242 (1984).
[13] Dawes, D. H., McPhedran, R. C., Whitbourn, L. B., “Thin capacitive meshes on a dielectric boundary: theory and experiment,” Applied Optics. 28(15), 3498-3510 (1989).
[14] Wurtz, G. A., Evans, P. R., Hendren, W., Atkinson, R., Dickson, W., Pollard, R. J., and Zayats, A. V., “Molecular plasmonics with tunable exciton-plasmon coupling strength in j-aggregate hybridized Au nanorod assemblies,” Nano Letters, 7(5), 1297-1303 (2007).
[15] Kavokin, A., Baumberg, J. J., Malpuech, G. and Laussy, F. P., [Microcavities], Oxford University Press, Oxford (2007).
[16] Ginn, J., Shelton, D., Krenz, P., Lail, B., and Boreman, G., “Altering infrared metamaterial performance through metal resonance damping,” Journal of Applied Physics, 105(074304), 074304-1-8 (2009).
[17] Wu, C., Khanikaev, A. B., Adato, R., Arju, N., Ali Yanik, A., Altug, H. and Shvets, G., "Fano-resonant asymmetric metamaterials for ultrasensitive spectroscopy and identification of molecular monolayers," Nature Material, 11, 69-75, (2012).
[18] Fano, U., “Effects of configuration interaction on intensities and phase shifts,” Physical Review, 124(6), 1866-1878 (1961).
[19] Papasimakis, N., Fedotov, V. A. and Zheludev, N. I., "Metamaterial analog of electromagnetically induced transparency," Physical Review Letters, 101( 25), 253903-1-4 (2008).
[20] Garrido Alzar, C. L., Martinez, M. A. G. and Nussenzveig, P., "Classical analog of electromegnetically induced transparency," American Journal of Physics, 70(1), 37-41 (2002).